Optics Communications 483 (2021) 126672

Contents lists available at ScienceDirect

Optics Communications

journal homepage: www.elsevier.com/locate/optcom

Development of a single-shot third-order cross-correlator for picosecond laser systems

A.C. Aiken [a,b], P. Oliveira [a], L.E. Bradley [a,*,1], E. Dilworth [c], M. Galletti [a,d,e], B. Parry [a], M. Galimberti [a], I.O. Musgrave [a]

[a] Central Laser Facility, STFC, Rutherford Appleton Laboratory, Harwell Campus, OX11 0QX, United Kingdom
[b] School of Mathematics and Physics, Queen's University Belfast, University Rd Belfast, BT7 1NN, United Kingdom
[c] Department of Mathematical Sciences, University of Bath, Bath BA2 7AY, United Kingdom
[d] GoLP Instituto de Plasmas e Fuso Nuclear, Instituto Superior Tecnico, Universidade de Lisboa, Av. Rovisco Pais 1049-001 Lisbon, Portugal
[e] INFN-LNF, Via Enrico Fermi 40, 00044 Frascati, Italy

ARTICLE INFO

Keywords:
Picosecond
Single shot
Third order cross correlator
Pulse characterisation

ABSTRACT

In this paper we present the development of a near-field single-shot third-order cross-correlator. We present measurements of sub-ps pulses at $\lambda = 1055.5$ nm demonstrating the device has a temporal window of $\Delta T = 36.4$ ps and a resolution of $\delta t = 91$ fs. We also discuss the spectral acceptance and the minimum required operational conditions.

1. Introduction

Since the advent of techniques such as chirped pulse amplification (CPA) [1] and optical parametric chirped pulse amplification (OPCPA) [2], petawatt class laser facilities have been developed to provide ultra-short pulses with petawatt peak power. These techniques offer attractive routes to explore light–matter interactions in the relativistic regime [3]. As the technologies producing ultra-short pulses have advanced, so too have the diagnostics used in characterising them. An extensive range of pulse characterisation methods have been reported within the field of laser science [4–8]. However, the majority of these methods have been focused on sub-100fs, large spectral bandwidth pulses, while the intermediate regime of ps pulses has seen fewer reported developments [9–11]. Despite this, picosecond and sub-picosecond pulses already possess a large range of applications, covering areas as diverse as medical applications in microsurgery [12,13], confocal and raman microscopy [14,15], material processing methods [16–18], terahertz pulse generation [19] and semiconductor testing [20].

Two instruments used widely in sub-ps petawatt class facilities for temporal characterisation and contrast measurements are single shot autocorrelators and scanning third-order cross-correlators (TOCC) respectively. [21,22] A general property of TOCC devices that is commonly utilised in high contrast applications is that the output signal scales cubically with the input signal, therefore changing the intensity by one order of magnitude will change the output signal by 10^3. As a result, they are often used in delay-scanning configurations over nanosecond scale time windows to detect amplified spontaneous emission (ASE), pre and post-pulses and the rise/fall times of laser pulses. However, scanning configuration measurements can be time consuming and not viable in an operational mode, especially for low repetition rate systems with significant shot to shot variation.

Single-shot TOCC devices have been proposed in several communications [23–25]. These can be used to capture temporal features instantly and may be used to measure pulse duration in an equivalent manner to a single shot autocorrelator (SSAC). However, the third order cross correlation is a more informative measurement than the intensity autocorrelation (IA) obtained from an SSAC. The symmetric nature of the IA means that little information about the pulse shape can be obtained. In addition, it is impossible to identify satellite pulses as post or pre-pulses using this measurement. By comparison, the third order cross correlation is an asymmetric measurement where the fundamental pulse is probed by the shorter second harmonic offering more information than a simple autocorrelation. This allows features preceding and following the main pulse to be resolved. An additional advantageous feature is the low noise present at the third-harmonic wavelength. This arises due to the absence of direct third harmonic generation processes occurring in the bulk of normally dispersive, isotropic, homogeneous media [26,27].

This proposal is based on developing a single shot TOCC with a non-collinear beam geometry, mixing a fundamental and second harmonic generation (SHG) beam inside a barium borate (BBO) crystal in a type

* Corresponding author.
E-mail address: laurence.bradley@stfc.ac.uk (L.E. Bradley).
[1] ORCID: https://orcid.org/0000-0001-7682-7221.

https://doi.org/10.1016/j.optcom.2020.126672
Received 12 August 2020; Received in revised form 23 November 2020; Accepted 1 December 2020
Available online 3 December 2020

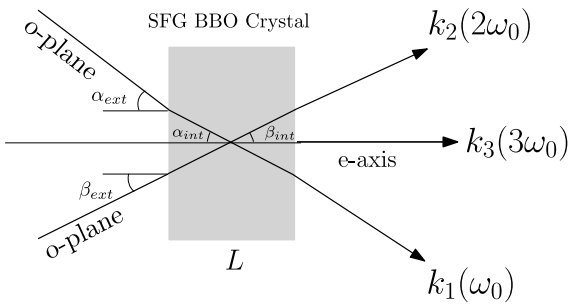

Fig. 1. Diagram showing the type-1 phase matching process in a sum frequency generating BBO crystal. The fundamental beam with wave vector k_1 and frequency ω_0 interacts with the crystal surface at an external angle α_{ext}, creating the internal angle α_{int} with the plane normal to the crystal surface. The second harmonic beam interacts with the crystal at β_{ext} and internal angle β_{int}. The two beams phase match at θ to produce sum frequency generated k_3 with three times the original frequency $3\omega_0$.

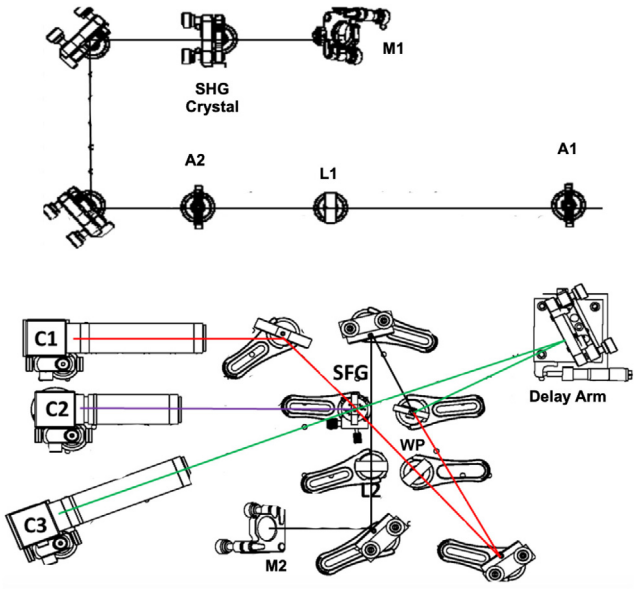

Fig. 2. Schematic showing a top-down view of the upper (top) and lower (bottom) decks of the single shot TOCC.

I phase matching process as shown in Fig. 1. This development is intended to be relevant to picosecond laser systems as a near-field (NF) diagnostic independent of the far-field (FF).

2. Design of the device

A schematic of the upper and lower decks of the device is presented in Fig. 2.

The input beam passes alignment apertures A1 and A2, with lens L1 of focal length $f_1 = 400$ mm placed in between. It then passes through a BBO crystal where a portion of the beam is co-linearly frequency doubled. The two pulses then propagate to the lower (M1 to M2) deck where they pass through lens L2 of focal length $f_2 = 400$ mm. Afterwards, the IR fundamental and SHG pulses are separated using a beam splitter that reflects the SHG pulses to a delay stage with the IR pulses being transmitted and reflected off a mirror. The TOCC signal is then generated by overlapping the SHG and IR signals in a non-collinear geometry in a SFG crystal. The non-collinear beam geometry allows the SFG beam, detected in camera C2 to be easily separated from the IR and SHG beams detected in camera C1 and C2 respectively. The detected TOCC signal is given by

$$TOCC(\tau) = \int_{-\infty}^{\infty} I^2(t-\tau)I(t)dt \tag{1}$$

where τ is the time delay, $I(t)$ is the IR beam intensity and $I^2(t-\tau)$ is the SHG beam intensity. The phase matching in both crystals is type I. Therefore, a $\lambda/2$ waveplate (WP) is placed in the fixed IR arm before the second BBO crystal to ensure the IR and SHG beam polarisations are vertical at the crystal. In order to optimise imaging and minimise beam pointing aberrations, the SFG beam must exit perpendicular to the surface of the crystal. To achieve this, the components of the light momenta of the two incident beams must balance each other due to momentum conservation. We describe this process as follows:

$$k_\omega \sin(\alpha_{int}) = k_{2\omega} \sin(\beta_{int}) \tag{2}$$

$$k_{3\omega} = k_\omega \cos(\alpha_{int}) + k_{2\omega} \cos(\beta_{int}) \tag{3}$$

where k_ω is the fundamental wave vector, $k_{2\omega}$ is the SHG wave vector, $k_{3\omega}$ is the SFG wave vector and α_{int} and β_{int} are the refracted angles of the IR and SHG beams inside the crystal determined from α_{ext} and β_{ext} using Snell's law. Both crystals are BBO, the measured thicknesses being $L_{SHG} = 1$ mm and $L_{SFG} = 100$ μm. The phase matching angle of the SFG crystal is $\theta = 76.2°$, requiring $\alpha_{ext} = 47°$ and $\beta_{ext} = 21.5°$ and by Snell's law $\alpha_{int} = 26.3°$ and $\beta_{int} = 12.6°$ for matching to occur.

The relay lens system (L1 and L2) makes the TOCC a NF device, insensitive to the direction of the entering beam provided it is within the numerical aperture of the device. Petawatt systems are complex and beam pointing deviations are common making this an important property.

In order to calculate the available time window on the device both the crystal and the camera chip size must be considered. However, the whole crystal can be imaged on camera C2 making it clear that the crystal size is the limiting factor. The non-collinear geometry converts the temporal domain to the spatial domain such that the single-shot time window is calculated as the delay between the 2 pulses at the aperture of the crystal

$$\Delta T = \frac{D_{CR}}{c}(\sin\alpha_{ext} + \sin\beta_{ext}) \tag{4}$$

where D_{CR} is the diameter of the face of the crystal and c is the speed of light in vacuum. $D_{CR} = 1$ cm which when used with the values given prior gives a time window of $\Delta T = 36.64$ ps. In order to increase the size of the time window, either the beam/crystal size or the angle between the beams must be increased. Increasing the latter would require a larger phase matching angle (and hence a different crystal).

To maximise the SFG signal the path length along each arm should be equal. The SH delay arm can be moved over a range of 25 mm to allow for correction and for the calibration of the delay scale in the detector. The delay at a given motor position is given by

$$\tau = \frac{2x_m \cos(\beta_{ext} + \theta_i)}{c}(\cos(\theta_i) - \sin(\theta_i)\tan(\beta_{ext})) \tag{5}$$

where x_m is the motor position and the beam angle of incidence on the delay mirror is θ_i The relation between the motor position and the position on C2 (x_c) is given by

$$\frac{x_c}{x_m} = 2M\cos(\beta + \theta_i)\sin(\theta_i)\cos(\beta) \tag{6}$$

where M is the magnification between the crystal and C2. The calibration factor, measured in px ps^{-1}, giving the temporal scale of measurements made by C2 is

$$C_F = \frac{c}{M p_{xL}} \frac{\cos\beta_{ext}}{\cot\theta_i - \tan\beta_{ext}} \tag{7}$$

where p_{xL} is the length of a single pixel on the camera chip.

The fundamental temporal resolution limit of the device is determined by the thickness of the crystal. This is expressed by

$$\delta t_f = L_{SFG} \frac{(\cos\beta_{int} - \cos\alpha_{int})}{c} \tag{8}$$

Using the values given prior, the temporal resolution of the TOCC due to the crystal is therefore $\delta t_f = 26.4$ fs. However, the temporal resolution of the device is also dependent on the camera temporal resolution, given by $\delta t_{cam} = 1/C_F$. Consequently, the larger of the pair of values is the true temporal resolution of the device.

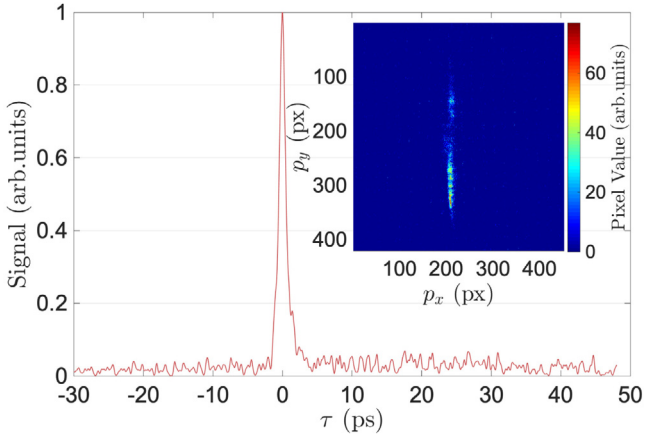

Fig. 3. TOCC profile of the pulse retrieved through the lineout of the trace image. The signal in arbitrary units, normalised to the maximum value, is plotted against time in picoseconds from the point of maximum signal. (Inset) Experimental result showing the single-shot measurement of the compressed millijoule OPCPA laser system [28].

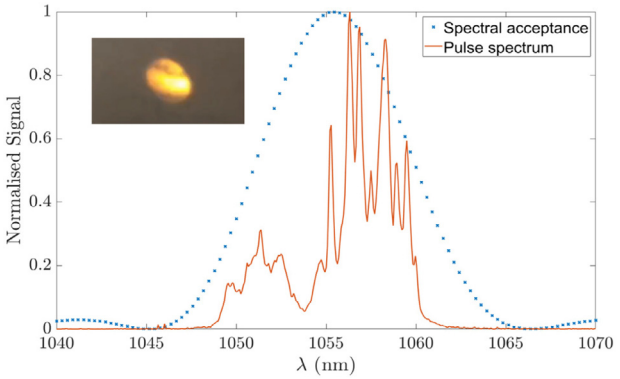

Fig. 4. Phase matching effects on the device. Spectrum of the beam entering the TOCC plotted against the spectral acceptance curve of the device. (Inset) Spatial profile of the SHG beam.

3. Experimental results

The device was tested using a partially compressed, sub-ps OPCPA beam with ∼1 cm diameter and energy ∼100 μJ. The instrument was used to observe visual features of the spatial profile. It was observed that this is highly dependent on the phase matching conditions found in the first SHG crystal. The horizontal uniformity of the spatial profile observed in the inset of Fig. 4 is the combined result of the crystal in the quasi-near field and the vertical SHG polarisation. In practical terms, the horizontal orientation and uniformity of the beam gives an increased SFG signal at lower energies and removes distortions along the time axis of the signal.

The experimental TOCC trace, observed on camera C2 as shown in the inset of Fig. 3 was collected by imaging the SFG crystal. By moving the delay arm shown in Fig. 2, the trace line on the camera was observed to move across the time window. M and p_{xL} for the device were 0.29 and 4.2 μm respectively which, upon substitution of M into (6) gave $\theta_i = 2.83°$. From this, the maximum time delay correction and calibration factor were therefore $\tau_{max} = 148$ and $C_F = 11.02$ px ps^{-1}. Using C_F, the camera temporal resolution was $\delta t_{cam} = 91$ fs, greater than δt_f, making δt_{cam} the temporal resolution of the TOCC. A plot of the TOCC trace as a function of delay after performing a horizontal lineout on the camera image is shown in Fig. 3. The full-width half-maximum of the TOCC was determined to be $\Delta t_{fwhm} = 1.33$ ps. Assuming a Gaussian pulse profile, the pulse duration was $\Delta t = 940$ fs.

The operational bandwidth of the device i.e. the spectral region where phase matching can occur, is limited by the effects of chromatic dispersion. To find the bandwidth $\Delta\Omega$ and verify that phase matching conditions were achieved, the spectral acceptance curve given by the product of the acceptance at both BBO crystals is plotted against the IR spectrum of the input beam in Fig. 4. The curve being considered also corresponds to the worst case scenario of a significantly chirped pulse. The width of the spectral acceptance region in Fig. 4 corresponds to the operational bandwidth. It was calculated to be $\Delta\Omega \sim 20$ nm. The bandwidth of the beam spectrum is notably smaller than the spectral acceptance region, thereby allowing phase matching conditions to be achieved across all wavelengths of the input beam.

4. Conclusion

Details on the development of a single-shot third-order cross-correlator have been presented. A pulse of length 940 fs and energy ∼100 μJ has been used to test the device. This NF diagnostic has an acceptance bandwidth of 20 nm, a temporal resolution of 91 fs and a temporal window of 36.64 ps. The device is ideal for operational use in petawatt class laser facilities, offering improved ultrashort pulse characterisation over standard autocorrelator setups.

CRediT authorship contribution statement

A.C. Aiken: Investigating,Writing - original draft, Software. **P. Oliveira:** Conceptualization, Software, Project administration, Writing - Review & Editing. **L.E. Bradley:** Investigation, Writing - original draft. **E. Dilworth:** Investigation. **M. Galletti:** Writing - Review & Editing. **B. Parry:** Methodology. **M. Galimberti:** Funding acquisition . **I.O. Musgrave:** Funding acquisition, Writing - Review & Editing.

Declaration of competing interest

The authors declare that they have no known competing financial interests or personal relationships that could have appeared to influence the work reported in this paper.

Acknowledgment

Funded by Central Laser Facility, Science and Technology Facilities Council (Part of UK Research and Innovation).

References

[1] Donna Strickland, Gerard Mourou, Compression of amplified chirped optical pulses, Opt. Commun. 56 (3) (1985) 219–221, http://dx.doi.org/10.1016/0030-4018(85)90120-8.

[2] I.N Ross, P. Matousek, M. Towrie, A.J Langley, J.L Collier, The prospects for ultrashort pulse duration and ultrahigh intensity using optical parametric chirped pulse amplifiers, Opt. Commun. 144 (1) (1997) 125–133, http://dx.doi.org/10.1016/S0030-4018(97)00399-4.

[3] C.P. Ridgers, J.G. Kirk, R. Duclous, T.G. Blackburn, C.S. Brady, K. Bennett, T.D. Arber, A.R. Bell, Modelling gamma-ray photon emission and pair production in high-intensity laser–matter interactions, J. Comput. Phys. 260 (2014) 273–285, http://dx.doi.org/10.1016/j.jcp.2013.12.007.

[4] J.A. Armstrong, Measurement of picosecond laser pulse widths, Appl. Phys. Lett. 10 (1) (1967) 16–18, http://dx.doi.org/10.1063/1.1754787.

[5] Rick Trebino, Frequency-resolved optical gating: the measurement of ultrashort laser pulses, Springer Science & Business Media, 2012.

[6] C. Iaconis, I.A. Walmsley, Spectral phase interferometry for direct electric-field reconstruction of ultrashort optical pulses, Opt. Lett. 23 (10) (1998) 792–794.

[7] V.V. Lozovoy, I. Pastirk, M. Dantus, Multiphoton intrapulse interference. IV. Ultrashort laser pulse spectral phase characterization and compensation, Opt. Lett. 29 (7) (2004) 775–777.

[8] M. Miranda, L.C. Arnold, T. Fordell, F. Silva, B. Alonso, R. Weigand, A. L'Huillier, H. Crespo, Characterization of broadband few-cycle laser pulses with the d-scan technique, Opt. Express 20 (17) (2012).

[9] K. Naganuma, K. Mogi, H. Yamada, General method for ultrashort light pulse chirp measurement, IEEE J. Quantum Electron. 25 (6) (1989) 1225–1233.
[10] Tzu-Ming Liu, Yin-Chieh Huang, Gia-Wei Chern, Kung-Hsuan Lin, Chih-Jie Lee, Yu-Chueh Hung, Chi-Kuang Sun, Triple-optical autocorrelation for direct optical pulse-shape measurement, Appl. Phys. Lett. 81 (8) (2002) 1402–1404, http://dx.doi.org/10.1063/1.1501453.
[11] Tzu-Ming Liu, Yin-Chieh Huang, Gia-Wei Chern, Kung-Hsuan Lin, Yu-Chueh Hung, Chih-Jie Lee, Chi-Kuang Sun, Characterization of ultrashort optical pulses with third-harmonic-generation based triple autocorrelation, IEEE J. Quantum Electron. 38 (11) (2002) 1529–1535.
[12] R.R. Anderson, J.A. Parrish, Selective photothermolysis: precise microsurgery by selective absorption of pulsed radiation, Science 220 (4596) (1983) 524–527.
[13] S.L Kilmer, R.R. Anderson, Clinical use of the Q-switched ruby and the Q-switched nd:YAG (1064 nm and 532 nm) lasers for treatment of tattoos, J. Dermatol. Surg. Oncol. 19 (4) (1993) 330–338.
[14] G.J. Puppels, F.F.M. de Mul, C. Otto, J. Greve, M. Robert-Nicoud, D.J. Arndt-Jovin, T.M. Jovin, Studying single living cells and chromosomes by confocal Raman microspectroscopy, Nature 347 (1990) 301–303, http://dx.doi.org/10.1038/347301a0.
[15] Khanh Kieu, Brian G. Saar, Gary R. Holtom, X. Sunney Xie, Frank W. Wise, High-power picosecond fiber source for coherent Raman microscopy, Opt. Lett. 34 (13) (2009) 2051–2053, http://dx.doi.org/10.1364/OL.34.002051.
[16] Petronic S., Sibalija T., Burzic M., Polic S., Colic K., Milovanovic D., Picosecond laser shock peening of nimonic 263 at 1064 nm and 532 nm wavelength, Metals 6 (3) (2016).
[17] Jan S. Hoppius, Lalit M. Kukreja, Marina Knyazeva, Fabian Pöhl, Frank Walther, Andreas Ostendorf, Evgeny L. Gurevich, On femtosecond laser shock peening of stainless steel aisi 316, Appl. Surf. Sci. 435 (2018) 1120–1124.
[18] Ludovic Rapp, Abdou Karim Diallo, Anne Patricia Alloncle, Christine Videlot-Ackermann, Frédéric Fages, Philippe Delaporte, Pulsed-laser printing of organic thin-film transistors, Appl. Phys. Lett. 95 (17) (2009) 171109, http://dx.doi.org/10.1063/1.3255011.
[19] K.-L. Yeh, M.C. Hoffmann, J. Hebling, Keith A. Nelson, Generation of 10 μ j ultrashort terahertz pulses by optical rectification, Appl. Phys. Lett. 90 (17) (2007) 171121.
[20] J.S. Melinger, S. Buchner, D. McMorrow, W.J. Stapor, T.R. Weatherford, A.B. Campbell, H. Eisen, Critical evaluation of the pulsed laser method for single event effects testing and fundamental studies, IEEE Trans. Nucl. Sci. 41 (6) (1994) 2574–2584.
[21] S. Luan, et al., High dynamic range third-order correlation measurement of picosecond laser pulse shapes, Meas. Sci. Technol. 4 (4) (1993).
[22] V.N. Ginzburg, et al., Third-order correlator for measuring the time profile of petawatt laser pulses, Quantum Electron. 38 (1027–1032) (2008).
[23] A. Kon, M. Nishiuchi, H. Kiriyama, K. Ogura, H. Sakaki, Y. Fukuda, M. Kando, K. Kondo, Single shot third-order cross-correlator for ultra-high intensity laser, in: 2015 11th Conference on Lasers and Electro-Optics Pacific Rim (CLEO-PR), Vol. 2, 2015, pp. 1–2.
[24] Jingui Ma, Yongzhi Wang, Peng Yuan, Guoqiang Xie, Heyuan Zhu, Liejia Qian, Single-shot pulse-contrast measurement based on high-order quasi-phase-matching cross-correlation, Opt. Lett. 37 (21) (2012) 4486–4488.
[25] I. Jovanovic, C. Brown, Constantin Haefner, Miro Shverdin, M. Taranowski, C.P.J. Barty, High-dynamic-range, 200-ps window, single-shot cross-correlator for ultrahigh intensity laser characterization, Conf. Lasers Electro-Opt. (2007) 1–2, http://dx.doi.org/10.1109/QELS.2007.4431082.
[26] G. Bjorklund, Effects of focusing on third-order nonlinear processes in isotropic media, IEEE J. Quantum Electron. 11 (6) (1975) 287–296.
[27] G.H.C. New, J.F. Ward, Optical third-harmonic generation in gases, Phys. Rev. Lett. 19 (1967) 556–559.
[28] B. Parry, P. Oliveira, A. Boyle, W. Shaikh, I. Musgrave, A new ns opcpa front end for vulcan petawatt, in: CLF Annual Reports, 2013-2014.